DOI 10.1007/s11182-020-02034-2

Russian Physics Journal, Vol. 63, No. 2, June, 2020 (Russian Original No. 2, February, 2020)

LOCALIZATION AND NATURE OF RADIATION DONOR DEFECTS IN THE ARSENIC IMPLANTED CdHgTe FILMS GROWN BY MBE

I. I. Izhnin,[1,2] O. I. Fitsych,[1] A. V. Voitsekhovskii,[2] A. G. Korotaev,[2] K. D. Mynbaev,[3] K. R. Kurbanov,[4] V. S. Varavin,[5] S. A. Dvoretskii,[5] N. N. Mikhailov,[5] V. G. Remesnik,[5] M. V. Yakushev,[5] O. Yu. Bonchyk,[6] H. V. Savytskyy,[6] Z. Świątek,[7] and J. Morgiel[7]

UDC 538.62, 548:537.611.46

By profiling the electrical parameters of the arsenic implanted CdHgTe *films, grown by molecular beam epitaxy, and comparing the obtained data with the results of studies performed by secondary ion mass spectroscopy and transmission electron microscopy, the localization and nature of donor defects formed during implantation were determined. It has been shown that such defects are dislocation loops and quasi-point defects that trap interstitial mercury atoms released during implantation.*

Keywords: CdHgTe, ion implantation, defects, electrophysical properties.

INTRODUCTION

CdHgTe solid solutions (MCT) are ones of the main materials of infrared photoelectronics [1]. Currently, the technology of high-temperature MCT–based photodetectors is actively developing. For such devices, the technology of «$p^+ - n$» type photodiodes is relevant, where the electronic type of conductivity of the initial n-base is obtained by doping with a donor impurity. As a result, the charge carrier lifetime in the base turns out to be limited by the non-radiative CHCC mechanism (recombination of an electron and a hole with excitation of another electron to a higher energy state), and the dark currents of photodiodes can be reduced by two orders of magnitude compared to the currents in «$n^+ - p$» structures, where, as a rule, monomolecular recombination dominates in the base.

The most common method for creating a p^+-region in n-type MCTs is ion implantation (II), and the most commonly used impurity is arsenic [2, 3]. The technology for the formation of p^+–n-junctions using arsenic II is more complex than the technology for the formation of «$n^+ - p$»-junctions in vacancy-doped MCTs. II in MCT leads to significant radiation damages, which is due to the low formation energies of intrinsic defects inherent in this material,

[1]Scientific Research Company "Electron-Carat", Lviv, Ukraine, e-mail: i.izhnin@carat.electron.ua; o_fitsych@ukr.net; [2]National Research Tomsk State University, Tomsk, Russia, e-mail: vav43@mail.tsu.ru; kor@mail.tsu.ru; [3]ITMO University, St. Petersburg, Russia, e-mail: mynkad@mail.ioffe.ru; [4]Kremenchug Flight College of the National Aviation University, Kremenchug, Ukraine, e-mail: kurbanovkurban424@gmail.com; [5]Rzhanov Institute of Semiconductor Physics of the Siberian Branch of the Russian Academy of Sciences, Novosibirsk, Russia, e-mail: varavin@isp.nsc.ru; dvor@isp.nsc.ru; mikhailov@isp.nsc.ru; remesnik@isp.nsc.ru; yakushev@isp.nsc.ru; [6]Ya. S. Pidstryhach Institute for Applied Problems of Mechanics and Mathematics of the National Academy of Sciences of Ukraine, Lviv, Ukraine, e-mail: bonchyk@ukr.net; grigorij.savitskij@gmail.com; [7]Institute of Metallurgy and Material Science of the Polish Academy of Sciences, Krakow, Poland, e-mail: z.swiatek@imim.pl; j.morgiel@imim.pl.
Translated from Izvestiya Vysshikh Uchebnykh Zavedenii, Fizika, No. 2, pp. 98–103, February, 2020. Original article submitted December 16, 2019.

 1064-8887/20/6302-0290 ©2020 Springer Science+Business Media, LLC

and regardless of the valency of the implanted impurity, the material after the II has an electronic type of conductivity due to the donor nature of the defects formed. Creating a p^+–n-structure with specified electrophysical parameters requires both annealing of radiation defects and electrical activation of introduced arsenic. To successfully solve these problems, knowledge of the nature and localization of defects introduced by implantation is necessary. The aim of this work was to determine the types of radiation donor defects, their spatial location, and nature in the arsenic implanted MCT epitaxial structure (ES) grown by molecular beam epitaxy (MBE).

1. EXPERIMENT

The initial $Cd_xHg_{1-x}Te$ ES was grown at the Rzhanov Institute of Semiconductor Physics SB RAS (Novosibirsk) on a (013) CdTe/ZnTe/Si substrate with *in situ* growth control using an automatic ellipsometer [4]. The composition of the active ES layer x_a was 0.22, the surface composition of the 0.4 μm thick graded-gap protective layer (GGPL) was 0.46, and the total thickness of the ES was 9.1 μm. The structure was *in situ* doped with indium with the calculated concentration of ~$6\cdot10^{15}$ cm^{-3}, so that after growing, it had n-type conductivity. In order to avoid "masking" the influence of radiation donor defects by the high electron conductivity of the n-type base layer, profiling of the electrical parameters was carried out on samples with the initial p-type conductivity. These samples were obtained by thermal annealing of ES in a helium atmosphere at low mercury vapor pressure (220°C, 24 h).

We investigated two similar samples - with the saved GGPL and with the removed one. The implantation of both samples was carried out in one cycle on an IMC200 setup (Ion Beam Services, France) by As^+ ions with an energy E = 190 keV and a fluence $F = 10^{15}$ cm^{-2} without activation annealing. The electrical properties of ESs were studied by measuring the field dependences of the Hall coefficient $R_H(B)$ and conductivity $\sigma(B)$ at 77 K in the range of magnetic fields of 0.01–1.2 T. To analyze the experimental dependences $R_H(B)$ and $\sigma(B)$ and determine the composition and parameters of charge carriers, we used the Discrete Mobility Spectrum Analysis (DMSA) method developed by the authors of [5]. Structural defects were investigated by transmission electron microscopy (TEM) in a bright field mode using a Tecnai G2 electron microscope (FEI Company). To prepare thin foils, we used a focused Ga^+ ion beam etching technique in the FEI Quanta 200 setup equipped with the Omniprobe™ lift-out sample handling system. The distribution profiles of the implanted ions were studied by secondary ion mass spectroscopy (SIMS) using a Cameca IMS-6F device (France) with an arsenic detection limit of ~10^{16} cm^{-3}.

2. RESULTS AND DISCUSSION

An analysis of the mobility spectra of the implanted ESs showed that the contribution to the conductivity was due to four types of charge carriers: electrons with high mobility (~90000 cm^2/(V·s)), two types of electrons with low mobility (~20000 cm^2/(V·s) and ~5000 cm^2/(V·s)), as well as heavy holes, with the dominant contribution of electrons. Thus, as a result of implantation, n^+–n–p-structures were formed, similar to those observed by the authors in p-type MCT after II of arsenic with fluences of 10^{12}–10^{15} cm^{-2} [6, 7]. In such structures, the p-region represents the remaining part of the initial p-type structure not modified by II, and the n^+–n-region characterizes the result of the II action, since the charge carriers observed in it are absent (or their contribution is negligible) in the initial structures both of p- and n-type. Table 1 shows the parameters of electrons in the ESs after the II, where σ_0 is the integral conductivity.

To determine the distribution of charge carriers over the depth of the implanted ESs, step-by-step chemical etching was carried out with the measurement of the dependences $R_H(B)$ and $\rho(B)$ after each etching step and their analysis by the DMSA method and determination of the number of carrier species and their parameters. For this, the implanted structures were divided into six samples. Chemical etching in a solution of 0.05% Br_2+HBr was carried out individually and once for each sample. The thickness of the removed layer was determined from the shift of the interference bands' extrema in the transmission spectra at 300 K. Figures 1 and 2 show evolution of the primary envelopes of the mobility spectra of samples with and without GGPL after the three (odd) etching steps. It is seen that the envelopes of the mobility spectra for these samples are, in principle, similar.

TABLE 1. Parameters of Electrons in Implanted ESs

Parameter of electrons	Sample with GGPL, $\sigma_0 = 29.4\ (\Omega\cdot cm)^{-1}$			Sample without GGPL, $\sigma_0 = 33.6\ (\Omega\cdot cm)^{-1}$		
	Average concentration, cm^{-3}	Mobility, $cm^2/(V\cdot s)$	Average partial conductivity, $(\Omega\cdot cm)^{-1}$	Average concentration, cm^{-3}	Mobility, $cm^2/(V\cdot s)$	Average partial conductivity, $(\Omega\cdot cm)^{-1}$
With high mobility	$4.85\cdot10^{14}$	97200	7.54	$5.06\cdot10^{14}$	90700	7.35
With an intermediate mobility	$5.95\cdot10^{14}$	23700	2.26	$8.28\cdot10^{14}$	18800	2.49
With low mobility	$2.34\cdot10^{16}$	4790	17.9	$3.02\cdot10^{16}$	4530	21.9

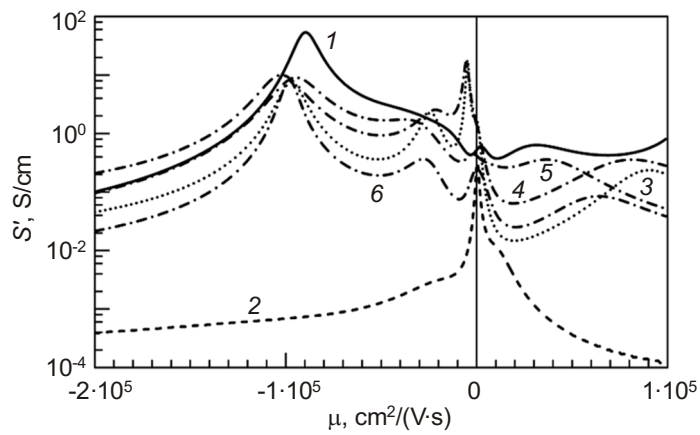

Fig. 1. Primary envelopes of the mobility spectra of the sample with a GGPL: *as-grown* (*n*-type) (*1*), after annealing (*p*-type) (*2*), after II (*3*), and after II and etching of layers with thicknesses of 0.12 μm (*4*), 0.46 μm (*5*), and 0.78 μm (*6*).

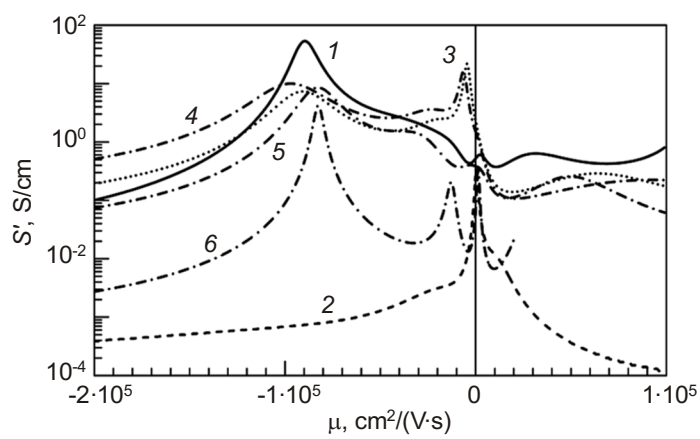

Fig. 2. Primary envelopes of the mobility spectra of the sample without a GGPL: *as-grown* (*n*-type) (*1*), after annealing (*p*-type) (*2*), after II (*3*), and after II and etching of layers with thicknesses of 0.32 μm (*4*), 0.54 μm (*5*), and 0.73 μm (*6*).

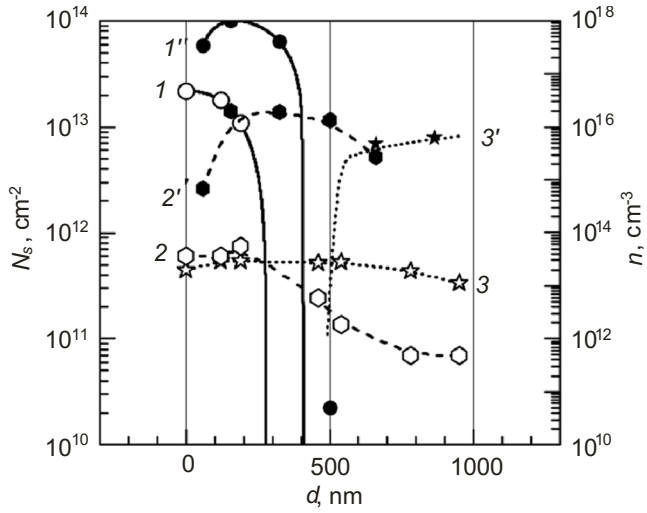

Fig. 3. Depth distribution of the sheet N_s (*1*, *2*, *3*) and bulk n (*1'*, *2'*, *3'*) concentrations of electrons with low (*1*, *1'*), intermediate (*2*, *2'*), and high (*3*, *3'*) mobility in the sample with a GGPL.

The shape of the envelopes after etching of about 300 nm indicates that the layer, in which electrons with low mobility make the dominant contribution to the conductivity, was removed (curves *4* and *5*). The parameters of electrons with high mobility changed little during etching, which suggests that the layer of material, in which these charge carriers dominate, is practically not affected by etching. As a result of the analysis of the mobility spectra envelopes for the samples subjected to chemical etching, the parameters of three types of electrons with different mobilities were determined: the mobility, average concentration, and partial conductivity (these parameters were calculated for the total thickness of the sample taking into account the etched layer).

The partial contribution of electrons with low mobility to σ_0 dominated after II and after etching the layer of a thickness of about 300 nm. At further etching, the partial conductivity caused by the contribution of these electrons sharply decreased. Similar changes were observed for the average concentration of these electrons. Thus, electrons with low mobility were localized to a depth of ~ 400 nm.

The parameters of electrons with high mobility, which are responsible for the conductivity in the *n*-region of the structure, remained almost constant during etching. After removal of the layer with a thickness of more than 400 nm, the partial conductivity of these electrons was dominant. Its noticeable decrease was observed only during the last etching steps, which could be associated with a decrease in the thickness of the *n*-region in the n^+–*n*–*p*-structure. Thus, spatially, *n*-region began at a depth of 700–800 nm. The formation of such a region in MCT during II and ion etching is a well-known fact [6–9]. The formation of this region is associated with the generation of interstitial mercury in the region of the radiation defect formation, its diffusion into the depth of the sample, and annihilation with the initial acceptor defects of the material — mercury vacancies. The electronic type of conductivity in this area after annihilation of these defects is determined by the residual or introduced donor impurities (in this case, indium).

To study the spatial distribution of various types of electrons and their partial conductivity, we calculated the values of the sheet concentrations and partial conductivities for each etching step and for each type of charge carriers. Then, the bulk electron concentrations and partial conductivities were calculated for each type of charge carriers. The results of the concentration profiling are shown in Figs. 3 and 4. Here, the points on the curves of the bulk electron concentration show the values calculated by differentiation over the points (values) of the sheet concentration. Lines are the approximating curves. We can also note here the similarity of the data obtained on the samples with and without GGPL.

The nature of the change in the average concentration and partial conductivity of electrons with intermediate mobility during etching was similar to that for electrons with low mobility. However, after removing a layer with

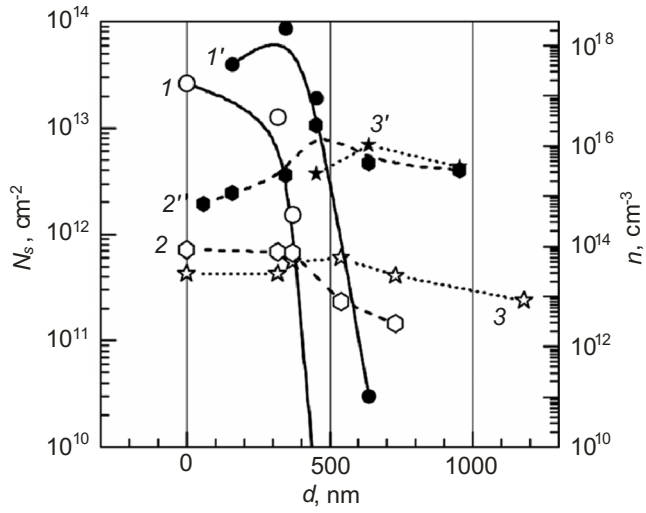

Fig. 4. Depth distribution of the sheet N_s (*1*, *2*, *3*) and bulk n (*1'*, *2'*, *3'*) concentrations of electrons with low (*1*, *1'*), intermediate (*2*, *2'*), and high (*3*, *3'*) mobility in the sample without a GGPL.

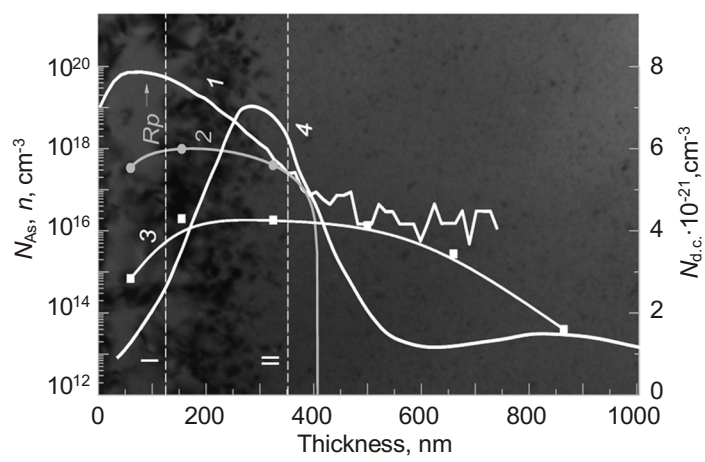

Fig. 5. Arsenic distribution profile according to SIMS data (*1*) and concentration profiles of electrons with low (*2*) and intermediate (*3*) mobility according to the measurement of electrical parameters superimposed on the TEM image of the cross section of the sample with a GGPL after implantation.

a thickness of 500 nm, the partial conductivity of the former exceeded that of the latter. Thus, the localization region of electrons with intermediate mobility extended to a depth of the order of 700–800 nm.

To draw conclusions about the nature of the origin of various types of charge carriers, the distribution profiles of the electron and implanted ion concentrations were superimposed on the TEM images of the cross section of the samples. For the sample with a GGPL, the superposition result is shown in Fig. 5. After II, the dominant contribution to the conductivity is made by electrons with low mobility (see Fig. 3, curve *1*) with a maximum concentration of ~10^{18} cm^{-3}. Figure 5 shows that they are localized in a layer containing implanted arsenic ions (curve *2*). In the same layer, extended radiation defects are localized, which were previously identified as dislocation loops [7].

Thus, the region of localization of electrons with low mobility extends to a depth of approximately 400 nm and coincides with the region of localization of implanted As ions (curve *1*) and extended structural defects (dislocation loops). It should be noted that during the ion etching of MCT, the formation of a damaged n^+-layer was also associated with the formation of dislocation loops and the conduction mechanism in it was associated with the formation of donor defects under trapping interstitial mercury atoms by loops [10]. Therefore, in case of II, we can assume that electrons with low mobility are due to similar donor centers.

As follows from curve *3* in Fig. 5, the region of localization of electrons with an intermediate mobility in the n^+-region extends to a depth of the order of 700–900 nm. Deeper than 400 nm, there are no extended defects capable of trapping interstitial mercury, so the appearance of these electrons must be due to other donor defects. Indeed, at depths greater than 350 nm, a uniform diffuse background is observed in the TEM image (below the II line in Fig. 5). This layer contains radiation quasi-point defects that were detected directly in Rutherford backscattering experiments in MCT samples subjected to arsenic II [11] (Fig. 5, curve *4*). That is, donor defects responsible for this type of electrons are complexes of interstitial mercury with other point defects.

CONCLUSIONS

Thus, a comparison of the data obtained by measuring the field dependences $R_H(B)$ and $\sigma(B)$ in combination with the step-by-step chemical etching and their analysis using the DMSA method with the TEM and SIMS data made it possible to detect and identify donor defects resulting from the ion implantation of arsenic in MCT ESs grown by MBE. In the *p*-type material, an n^+–*n*-structure was formed as a result of II. In its n^+–*n*-region, three types of electrons with different mobilities caused by the corresponding donor defects were detected. Electrons with a low mobility of the order of 5000 $cm^2/(V\cdot s)$ are localized in the near-surface n^+-layer with a thickness of ~400 nm, where extended structural defects — dislocation loops — are located. The donor center, which determines the presence of electrons with low mobility, is a defect based on the interstitial mercury atom captured by such a loop. Electrons with an intermediate mobility of ~20000 $cm^2/(V\cdot s)$ are also localized in the n^+-layer, in the region extending to a depth of 700–900 nm, where quasi-point radiation defects exist. Here, the donor defects are complexes formed by atoms of interstitial mercury with other point defects. Electrons with a high mobility of ~90000 $cm^2/(V\cdot s)$ are localized in the *n*-layer at a depth of more than 700–900 nm. The formation of this region is associated with the diffusion of interstitial mercury generated during implantation and its annihilation with mercury vacancies in the *p*-type material. The electronic conductivity of this region is determined by the residual or introduced donor impurities inherent in the initial sample.

REFERENCES

1. W. Lei, J. Antoszewski, and L. Faraone, Appl. Phys. Rev., **2**, No. 4, 041303 (2015).
2. N. Baier, C. Cervera, O. Gravrand, *et al*., J. Electron. Mater., **44**, No. 9, 3144–3150 (2015).
3. O. Gravrand and G. Destefanis, Infr. Phys. Technol., **59**, 159–171 (2013).
4. V. S. Varavin, V. V. Vasiliev, S. A. Dvoretsky, *et al*., Opto-Electron. Rev., **11**, No. 2, 99–111 (2003).
5. V. V. Bogoboyashchyy, A. I. Elizarov, and I. I. Izhnin, Semicond. Sci. Technol., **20**, No. 8, 726–732 (2005).
6. I. I. Izhnin, A. V. Voitsekhovsky, A. G. Korotaev, *et al*., Infr. Phys. Technol., **81**, No. 3, 52–58 (2017).
7. I. I. Izhnin, E. I. Fitsych, A. V. Voitsekhovsky, *et al*., Russ. Phys. J., **60**, No. 10, 1752–1757 (2018).
8. G. A. Umana-Membreno, H. Kala, J. Antoszewski, *et al*., J. Electron. Mater., **42**, No. 11, 3108–3113 (2013).
9. H. Ebe, M. Tanaka, and Y. Miyamoto, J. Electron. Mater., **28**, No. 6, 854–857 (1999).
10. I. I. Izhnin, K. D. Mynbaev, A. V. Voitsekhovsky, *et al*., Opto-Electron. Rev., **25**, No. 2, 148–170 (2017).
11. C. Lobre, D. Jalabert, I. Vickridge, *et al*., Nucl. Instrum. Meth. Phys. B, **313**, 76–80 (2013).